SCIENCE CHINA
Technological Sciences

Special Topic: Mechanics of Micro-nanostructured Materials
•Article•

January 2021 Vol.64 No.1: 11–22
https://doi.org/10.1007/s11431-020-1660-8

Dynamic recrystallization-induced temperature insensitivity of yield stress in single-crystal $Al_{1.2}CrFeCoNi$ micropillars

HUANG RuiRui[1], ZHANG Qian[1], ZHANG Xuan[1], LI JianGuo[1], CAO TangQing[2], YAO JiaHao[3], XUE YunFei[2*], GAO HuaJian[4,5*] & LI XiaoYan[1*]

[1] *Center for Advanced Mechanics and Materials, Applied Mechanics Laboratory, Department of Engineering Mechanics, Tsinghua University, Beijing 100084, China;*
[2] *School of Materials Science and Engineering, Beijing Institute of Technology, Beijing 100081, China;*
[3] *Shenyang National Laboratory for Materials Science, Institute of Metal Research, Chinese Academy of Sciences, Shenyang 110016, China;*
[4] *School of Mechanical and Aerospace Engineering, College of Engineering, Nanyang Technological University, Singapore 639798, Singapore;*
[5] *Institute of High Performance Computing, A*STAR, Singapore 138632, Singapore*

Received February 12, 2020; accepted May 29, 2020; published online July 27, 2020

High-entropy alloys, a new class of metallic materials, exhibit excellent mechanical properties at high temperatures. In spite of the worldwide interest, the underlying mechanisms for temperature dependence of mechanical properties of these alloys remain poorly understood. Here, we systemically investigate the mechanical behaviors and properties of $Al_{1.2}CrFeCoNi$ (comprising a body-centered cubic phase) and $Al_{0.3}CrFeCoNi$ (comprising a face-centered cubic phase) single-crystal micropillars with three orientations ([100], [110], and [111]) at temperatures varying from 300 to 675 K by using *in situ* compression of micropillars inside a scanning electron microscope. The results show that the yield stresses of $Al_{1.2}CrFeCoNi$ micropillars are insensitive to temperature changes, and their flow stresses and work hardening rates increase slightly with increasing temperature from 300 to 550 K, which differs from the typical temperature dependence of yield/flow stresses in metals and alloys. In contrast, $Al_{0.3}CrFeCoNi$ micropillars exhibit typical thermal softening. Furthermore, it is found that the $Al_{1.2}CrFeCoNi$ micropillars exhibit a transition from homogenous deformation to localized deformation at a critical temperature, while the $Al_{0.3}CrFeCoNi$ micropillars always maintain a well-distributed and fine slip deformation. Detailed transmission electron microscopy analyses reveal that dynamic recrystallization (involving dislocation tangles, and formation of dislocation cell structures and sub-grains) plays a key role in the observed temperature insensitivity of the yield stress and increasing flow stress (and work hardening rate) with increasing temperature in the $Al_{1.2}CrFeCoNi$ micropillars, and that thermally activated dislocation slip leads to thermal softening of the $Al_{0.3}CrFeCoNi$ micropillars. The differences in deformation modes and temperature dependence of the mechanical properties between $Al_{1.2}CrFeCoNi$ and $Al_{0.3}CrFeCoNi$ essentially originate from the differences in dislocation activities and slip systems since the two alloys adopt different phases. Our findings provide key insights in the temperature dependence of mechanical properties and deformation behaviors of high-entropy alloys with body-centered cubic and face-centered cubic phases.

high entropy alloy, temperature insensitivity, dynamic recrystallization, micropillar, deformation twin

Citation: Huang R R, Zhang Q, Zhang X, et al. Dynamic recrystallization-induced temperature insensitivity of yield stress in single-crystal $Al_{1.2}CrFeCoNi$ micropillars. Sci China Tech Sci, 2021, 64: 11–22, https://doi.org/10.1007/s11431-020-1660-8

*Corresponding authors (email: xueyunfei@bit.edu.cn; huajian.gao@ntu.edu.sg; xiaoyanlithu@tsinghua.edu.cn)

1 Introduction

High-entropy alloys (HEAs) are a new class of metallic materials that have revolutionized alloy design over the past decade [1–4]. HEAs generally consist of five or more elements with equal or nearly equal atomic concentrations of each element and are therefore also called multiprincipal element alloys [5,6]. Interestingly, HEAs exhibit four unique effects, including a high configurational entropy, severe lattice distortion, sluggish diffusion and cocktail effects [3,7,8]. In recent years, HEAs have attracted worldwide attention due to their exceptional mechanical properties, including high hardness/strength, good ductility, high fracture toughness, excellent thermal and refractory properties, and remarkable resistance to wear, friction and corrosion [7–11]. As a typical example of HEAs, $Al_xCrFeCoNi$ has been extensively studied for more than ten years [4,12–14]. The phase composition, microstructure and mechanical properties of this alloy can be tuned by changing the Al content x [12–14]. As x increases, the structure of the HEA transforms from face-centered cubic (FCC) to body-centered cubic (BCC), and its hardness and strength increase with x [12]. When x is smaller than 0.5, the $Al_xCrFeCoNi$ alloy comprises a single solid solution FCC phase. If x is larger than 0.9, it comprises a BCC phase only. When x falls between 0.5 and 0.9, it consists of a mixture of the FCC and BCC phases [12].

In modern industry, metallic structures and devices are widely used in various elevated temperature environment; thus, extensive studies on the temperature dependence of the mechanical properties of metallic materials are often required. Generally speaking, the mechanical properties (especially strength and fracture toughness) of metallic materials are dependent on the ambient temperature [11,15], since the deformation mechanisms and/or microstructure of materials are often temperature-dependent. Previous studies [16,17] have shown that the yield stress of BCC metals has a strong temperature dependence/sensitivity, i.e., as the temperature rises, the yield stress of BCC metals (including bulk samples and micropillars) decreases significantly. Such a strong temperature dependence/sensitivity is attributed to the thermal activation of dislocation nucleation and motion [18]. Interestingly, for BCC metal pillars, the temperature sensitivity decreases with a reduction in the pillar diameter [18]. This phenomenon arises from a mechanism transition from thermally activated kink activities to phonon-drag dislocation activities. It has also been noted that the temperature sensitivity nearly vanishes when the pillar diameter is reduced below approximately 200 nm [18]. Recently, for some BCC HEAs (including $Al_xCrFeCoNi$ with x>1.0, NbMoTaW, and VNbMoTaW) with high melting points, it was found that their yield or flow stresses exhibit a unique temperature dependence [14,19] that is different from those of pure metals and conventional alloys. When the temperature is lower than a critical value (which is dependent on the melting point T_m of the HEA), the yield/flow stress slowly decreases with increasing temperature, indicating a weak temperature dependence [20]. However, at temperatures above the critical value, the yield/flow stress rapidly decreases with increasing temperature. The weak temperature dependence below the critical temperature is thought to be attributed to severe lattice distortion [20] and slow atomic diffusion [19], while the apparent temperature dependence above the critical temperature can be related to the thermal activation of dislocation activities. To date, the underlying deformation mechanisms for the weak temperature dependence in BCC HEAs remain poorly understood.

In this paper, we investigate the temperature dependence of the mechanical responses and behaviors (such as the yield and flow stresses and work hardening rates) of BCC HEAs. In particular, single-crystal $Al_{1.2}CrFeCoNi$ micropillars with the BCC phase are studied, since the yield stress of this alloy in bulk form exhibits a weak temperature dependence. Single-crystal FCC $Al_{0.3}CrFeCoNi$ micropillars are used for comparison. The micropillars have three typical orientations, namely, [100], [110] and [111]. To reveal the underlying mechanisms responsible for the weak temperature dependence, we conduct *in situ* scanning electron microscopy (SEM) compressive tests on the micropillars and detailed transmission electron microscopy (TEM) observations.

2 Methods

2.1 Sample preparation and microstructural characterization

The $Al_{1.2}CrFeCoNi$ and $Al_{0.3}CrFeCoNi$ HEAs were synthesized by arc melting Al, Cr, Fe, Co, and Ni powders (>99.8% purity) under a high-purity argon atmosphere. During the synthesis process, the ingots were triple melted to ensure chemical homogenization. The HEA ingots were cast into a rectangular copper mold. For $Al_{1.2}CrFeCoNi$ with BCC phase, the as-cast samples were heated at 1200°C for 24 h for the reduction in the elemental segregation. For $Al_{0.3}CrFeCoNi$ with FCC phase, in order to reduce the elemental segregation and obtain equiaxed grain structures, the as-cast samples were heated at 1200°C for 24 h and then treated by cold rolling to achieve a 60% reduction in thickness and further annealing at 950°C for 1 h. We conducted XRD (Bruker D8 Advance) analysis to obtain the lattice constant and phase composition. The elemental compositions and orientation of the HEA specimens were determined with a scanning electron microscope (FEI Nova Nano430) that was equipped with energy dispersive spectrometry (EDS) and EBSD capabilities, respectively. According to the orientation maps, we fabricated single-crystal micropillars with a diameter of about 1200 nm and three types of or-

ientations, namely [100], [110] and [111], with a FIB-SEM system (LYRA3 TESCAN) [21]. During fabrication, all the micropillars were first milled by using a voltage and current of 30 kV and 1 nA, respectively, and finally polished with a voltage and current of 30 kV and 50 pA, respectively. All the micropillars had an aspect ratio (height/diameter) of about 2.5–3.5 and a taper of less than 3°. The TEM samples were fabricated by FIB milling (FEI Helios NanoLab 600i). Before milling, the micropillars were sputtered with platinum for protection. High-resolution TEM observations were conducted inside a transmission electron microscope (FEI TECNAI G2 F20) with an accelerating voltage of 300 kV.

2.2 *In situ* SEM compression

In situ compressive tests on micropillars were performed at 300, 425, 550, and 675 K inside a scanning electron microscope (Quanta FEG450) equipped with a Hysitron PI 85 PicoIndenter that included a thermal module. The diameter of the diamond flat punch used in the PicoIndenter was 5 μm. High temperatures were achieved by a MEMS heating device integrated in the thermal module of the PI 85. Before testing at high temperatures, the temperature was gradually increased to a prescribed value and then maintained at this value for 30 min to ensure that the tested sample reached the desired temperature. Throughout compression, the temperature was always kept at the prescribed value. After compression, the sample was naturally cooled to room temperature in vacuum for several hours. During compression, a constant strain rate of 10^{-3} s^{-1} was used. Each pillar was loaded to a maximum strain of 60%.

3 Results and discussion

3.1 Microstructural characterization and fabrication of the micropillars

Figure 1(a) and (b) show the X-ray diffraction (XRD) spectra of the $Al_{1.2}CrFeCoNi$ and $Al_{0.3}CrFeCoNi$ specimens, respectively. The results indicate that the $Al_{1.2}CrFeCoNi$ HEA is composed of the BCC phase (A2+B2, disordered and ordered BCC), while the $Al_{0.3}CrFeCoNi$ HEA is composed of the FCC phase. The formation of the A2+B2 phase in the $Al_{1.2}CrFeCoNi$ HEA is related to spinodal decomposition at high temperatures [22]. Figure 1(c) and (d) present the electron back scatter diffraction (EBSD) analyses of the $Al_{1.2}CrFeCoNi$ and $Al_{0.3}CrFeCoNi$ specimens, respectively. It is seen in Figure 1(c) and (d) that both $Al_{1.2}CrFeCoNi$ and $Al_{0.3}CrFeCoNi$ HEAs consist of fine and equiaxed grains. The mean grain size of the $Al_{1.2}CrFeCoNi$ HEA varies from tens to hundreds of micrometers, while that of the $Al_{0.3}CrFeCoNi$ HEA is hundreds of micrometers. According to the EBSD maps, we selected specific grains with grain sizes of hundreds of micrometers to fabricate a large number

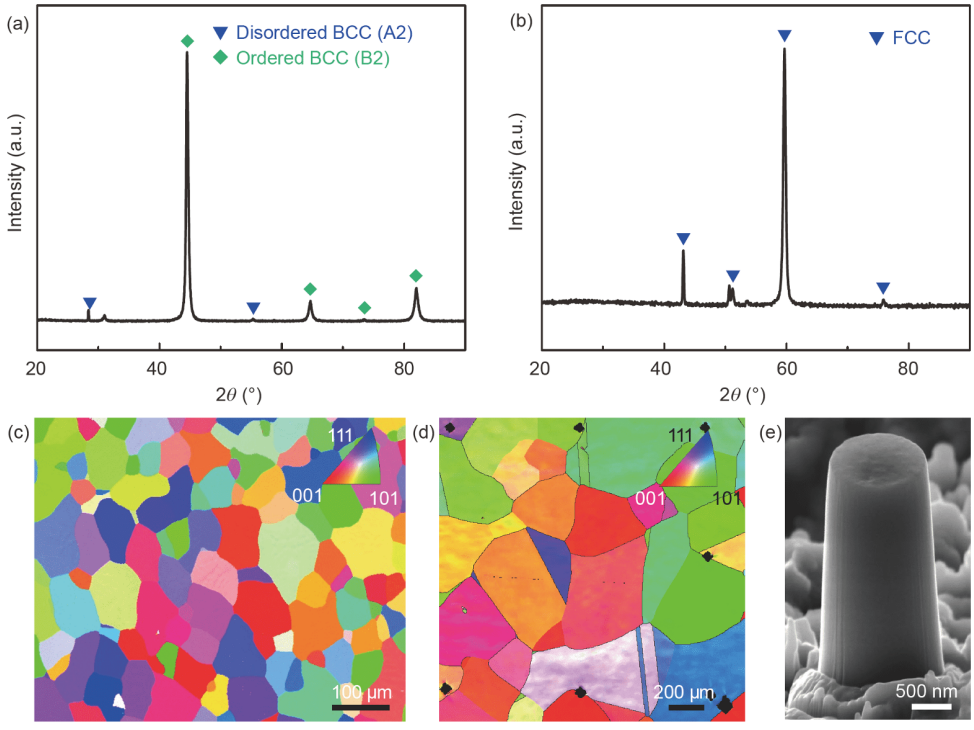

Figure 1 (Color online) Microstructural characterization of the $Al_{1.2}CrFeCoNi$ and $Al_{0.3}CrFeCoNi$ specimens and SEM images of typical micropillars. (a), (b) XRD spectra of the $Al_{1.2}CrFeCoNi$ and $Al_{0.3}CrFeCoNi$ specimens, respectively. The results indicate that the $Al_{1.2}CrFeCoNi$ HEA has an ordered and disordered BCC phase (A2+B2), while the $Al_{0.3}CrFeCoNi$ HEA has an FCC phase. (c), (d) Typical EBSD maps of the $Al_{1.2}CrFeCoNi$ and $Al_{0.3}CrFeCoNi$ HEAs, respectively. (e) SEM image of fabricated [100]-oriented $Al_{1.2}CrFeCoNi$ micropillar with a diameter of about 1.2 μm.

of single-crystal micropillars with diameters of about 1200 nm and orientations of [100], [110] and [111]. Figure 1 (e) shows a representative SEM image of the fabricated micropillars.

3.2 Temperature dependence of the mechanical behaviors and properties of the HEAs

To explore the temperature dependence of the mechanical behaviors and properties of the HEAs, we performed a series of *in situ* SEM compressive tests on the $Al_{1.2}$CrFeCoNi and $Al_{0.3}$CrFeCoNi micropillars at temperatures varying from 300 to 675 K. Figure 2(a) shows the representative stress-strain curves of the $Al_{1.2}$CrFeCoNi micropillars with three orientations at different temperatures. All micropillars initially undergo elastic deformation, followed by plastic yielding and apparent strain hardening, where the stress significantly increases with increasing of applied strain. It is noted that the stress-strain curves are smooth and continuous despite a few slight stress drops around the yielding condition. Figure 2(a) shows that the stress level of the micropillars at a given strain does not monotonically change with

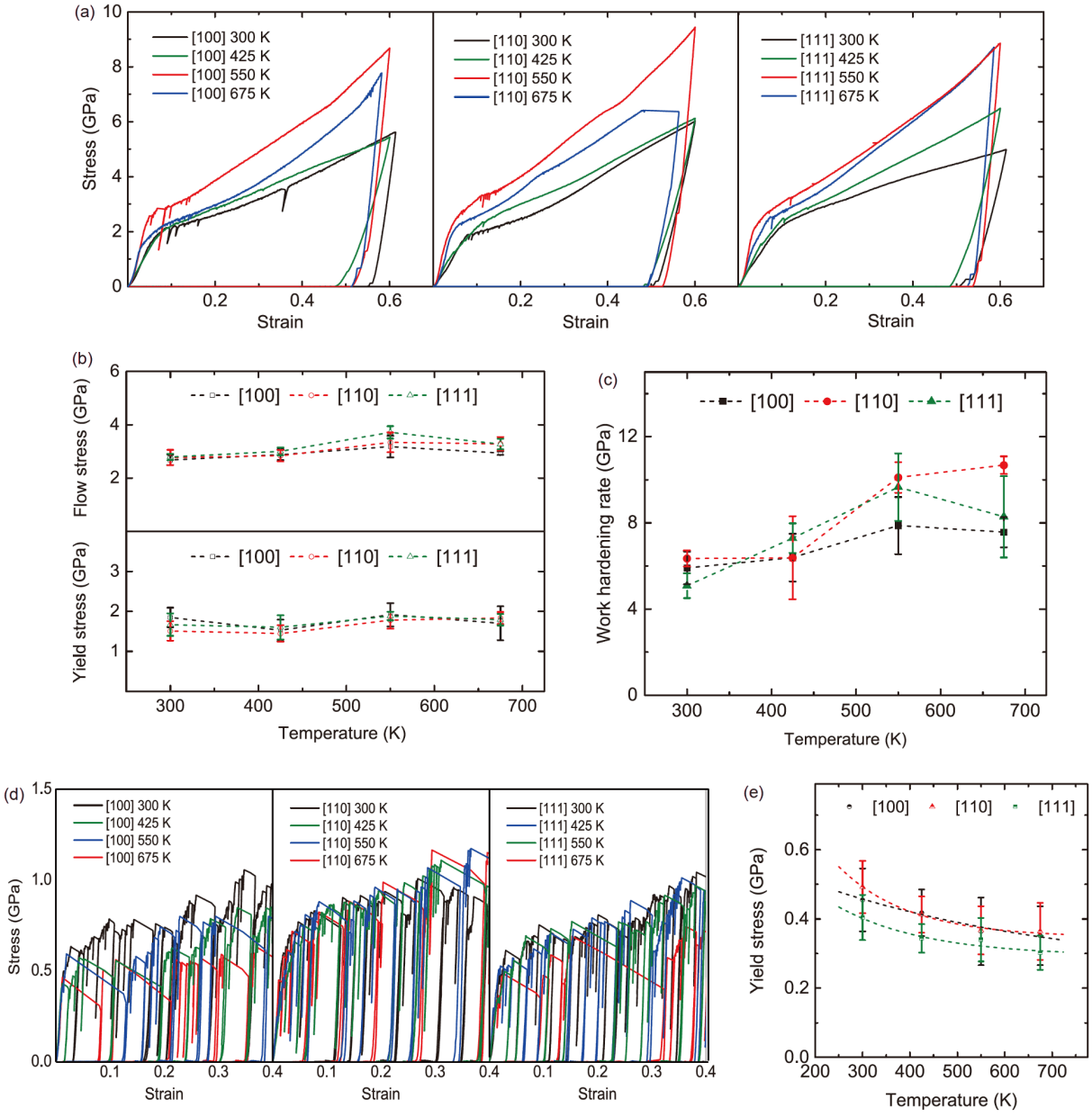

Figure 2 (Color online) Stress-strain curves and temperature dependences of the mechanical properties of the $Al_{1.2}$CrFeCoNi and $Al_{0.3}$CrFeCoNi micropillars. (a) Representative stress-strain curves of the $Al_{1.2}$CrFeCoNi micropillars with different orientations; (b) variations in the flow and yield stresses with temperature in the $Al_{1.2}$CrFeCoNi micropillars; (c) variation of the work hardening rate with temperature in the $Al_{1.2}$CrFeCoNi micropillars; (d) representative stress-strain curves of the $Al_{0.3}$CrFeCoNi micropillars with different orientations at different temperatures; (e) variation of the yield stress with temperature in the $Al_{0.3}$CrFeCoNi micropillars. The lines in (b) and (c) are used as a guide for the eye, while the lines in (e) are fitting curves based on eq. (1).

increasing temperature. Here, we chose two featured stresses: one is the 0.2% offset yield stress, and the other is the flow stress at the strain of 0.2, and we further characterized the influence of temperature on these two stresses. For each orientation and temperature, we tested at least 5 micropillars. Figure 2(b) plots the variations in the average yield and flow stresses (each data point was averaged over at least 5 tested samples) with the temperature. Strikingly, both the yield and flow stresses are insensitive to temperature change. In particular, nearly no strength softening occurs with increasing temperature from 300 K to 675 K, while the flow stress increases slightly (by 18.7%–33.0%) in the range from 300 K to 550 K (Figure 2(b)). This phenomenon is distinct from the weak temperature dependence of the yield stress observed in some BCC HEAs [19,20,23]. It is noted that previous experimental measurements gave a critical temperature (for the transition in the temperature dependence of the yield stress) of 903 K for the $Al_{1.2}$CrFeCoNi [14]. The temperature used in our experiment is lower than this critical temperature. It is noted that the sample size has no significant influence on the temperature dependence of mechanical properties, and that the current HEA micropillars with the diameter of 1200 nm have the similar temperature dependence of mechanical properties with the bulk samples. Therefore, for the $Al_{1.2}$CrFeCoNi micropillars, when the test temperature is below 903 K, the yield stress has the weak temperature dependence, indicating the temperature insensitivity. Otherwise, the yield stress significantly decreases with the increasing of test temperature, indicating the thermal softening. According to speculation from previous studies [20], the temperature insensitivity of the yield stress is likely related to lattice distortion and sluggish diffusion. However, these mechanisms cannot be used to account for the increase in flow stress with increasing temperature that we observed above, because these mechanisms only provide resistance to strength softening as the temperature rises. Subsequently, we further conducted detailed TEM observations and thorough analyses to reveal the deformation mechanisms responsible for the temperature insensitivity of the yield and flow stresses.

Furthermore, we analyzed the temperature dependence of the work hardening rate of the HEA micropillars. The work hardening rate was obtained by fitting the slope of the stress-strain curve between 10% and 40% strains. The work hardening rate of the micropillars at room temperature reached 5.09–6.35 GPa, which is higher than those (3.0–3.5 GPa) for BCC metal micropillars [24,25] but is comparable to those (3.5–4.5 GPa) for HEA micropillars [4]. Such phenomenon indicates that BCC HEAs under compression have the stronger working hardening capability than BCC metals [26]. Such strong working hardening capability is related to complex dislocation slip and dislocation tangle in BCC HEAs under compression, which originates from multi-principal elements and distorted lattice of BCC HEAs [26]. Figure 2(c) shows the variation in the work hardening rate of the micropillars with temperature. Despite the significant scatter, it can be seen in Figure 2(c) that the work hardening rate roughly increases with increasing temperature, which is consistent with reports for bulk BCC metals, where screw dislocations easily slip at high temperatures, giving rise to dislocation forest hardening [27]. This trend is similar to the temperature dependence of the flow stress. These results indicate that the temperature dependence of the work hardening rate and flow stress originate from the same mechanisms. It is noted that for a given temperature, both the yield and flow stresses of the micropillars with different orientations have apparent scatters. A similar phenomenon was observed during *in situ* compression of BCC Fe micropillars [28] and is related to the randomness of the dislocation sources and initial dislocations in the micropillars [28].

Figure 2(d) presents typical compressive stress-strain curves for the single-crystal $Al_{0.3}$CrFeCoNi micropillars with different orientations at different temperatures. Abrupt stress drops and strain bursts occur frequently in the stress-strain curves (Figure 2(d)). Such a phenomenon is commonly observed in FCC metal micropillars [29] but differs from the continuous and smooth variation of stress-strain curves (Figure 2(a)) of BCC HEA micropillars, indicating that dislocation slip in FCC micropillars is much easier than that in BCC micropillars. As the temperature increases from 300 K to 675 K, we observed an elevated strain burst and a decreased yield stress in the stress-strain curves due to thermal activation of the dislocation motion. We took the stress at the first large strain burst in the stress-strain curve as the yield stress of the FCC HEA micropillars and plotted it as a function of temperature in Figure 2(e). For all three orientations, the yield stress always decreases with increasing temperature, exhibiting common thermal softening. Considering the temperature-dependent lattice friction on the dislocation motion, previous studies developed an approximate expression that describes the temperature dependence of the yield stress in equi-atomic solid solution alloys with FCC phases. This expression is [30]

$$\sigma_y = \sigma_a \exp\left(-\frac{T}{C}\right) + \sigma_b, \tag{1}$$

where σ_y is the yield stress, T is the temperature, σ_a is the Peierls stress at 0 K, σ_b represents the athermal part associated with dislocation multiplication, and C is the effective temperature related to the Burgers vector and width of the dislocations. We used eq. (1) to fit our experimental data and plotted the fitting curves in Figure 2(e), with the fitting parameters listed in Table 1. It is seen in Figure 2(e) that the predictions based on eq. (1) agree well with our experimental data, indicating that the apparent temperature dependence of the yield stress in the FCC HEA micropillars is due to

Table 1 Values of parameters in eq. (1) by fitting our experimental data about $Al_{0.3}CrFeCoNi$ micropillars via eq. (1)

	σ_a (GPa)	σ_b (GPa)	C (K)
[100]-oriented	0.382	0.236	553
[110]-oriented	1.082	0.347	150
[111]-oriented	0.536	0.293	188

thermal activation of dislocation motion, where the temperature-dependent lattice friction is dominant. It is noted that for HEAs, the solid solution and resultant lattice distortion reduce the temperature dependence of the yield stress to an extent since they increase the barrier for dislocation motion [30].

3.3 Plastic deformation morphology analysis

Figure 3(a)–(c) show a sequence of SEM images of representative compressed [100]-, [110]- and [111]-oriented $Al_{1.2}CrFeCoNi$ micropillars, respectively, as the temperature increases from 300 K to 675 K. Regardless of the orientation, all $Al_{1.2}CrFeCoNi$ micropillars exhibit a homogenous and wavy deformation appearance at temperatures below 675 K, with some traces on the free surface, indicating the activation of the cross-slip of screw dislocations [31,32]. At 675 K, all $Al_{1.2}CrFeCoNi$ micropillars exhibit shear localization due to slip bands penetrating the micropillars, indicating that dislocation avalanches are induced by the activation of only a few slip systems at high temperatures [31,32]. Figure 3(a)–(c) implies a transition from homogenous to localized deformation in the single-crystal $Al_{1.2}CrFeCoNi$ micropillars with increasing temperature. Such a transition has been reported in previous compressive experiments on BCC metal micro/nanopillars [32]. This can be explained by the mobility of screw and edge dislocations, which is a function of the ratio of T/T_c, where T is the test temperature and T_c is the critical temperature [31]. For BCC metals/alloys, the critical temperature T_c is defined as the temperature at which the screw and edge dislocations have equal mobility [31]. When T/T_c is less than a critical value α_c (generally lower than 1), screw dislocations move slower than edge dislocations due to their nonplanar and polarized core structure [33,34]. Consequently, the edge dislocations move rapidly towards the free surface, escape from it and then produce a situation of edge dislocation starvation [31]. At the same time, a large number of screw dislocations cross slip, dominating the plastic deformation and leading to a homogenous and wavy deformation appearance (Figure 3 (a)–(c)) [31]. When T/T_c exceeds α_c, the edge and screw dislocations have comparable mobility because of the thermal activation of the screw dislocations that leads to an accumulation of mixed dislocations, in particular slip planes, and eventually a localized avalanche slip (Figure 3(a-4), (b-4) and (c-4)) [31].

Figure 3(d) shows the deformation morphologies of compressed [110]-oriented $Al_{0.3}CrFeCoNi$ micropillars at different temperatures. For all test temperatures, a large number of well-distributed fine slip steps occur on the free surface, and some slip traces even intersect, indicating that both surface dislocation nucleation and multiple slip systems are activated in the micropillar. This type of deformation morphology is frequently observed during compression of FCC metal/alloy micro/nanopillars [29,30] but differs from those (Figure 3(a)–(c)) of $Al_{1.2}CrFeCoNi$ micropillars in the BCC phase. The difference in the deformation morphology between the FCC and BCC HEA micropillars arises from the differences in dislocation activities and slip systems. Similar deformation morphologies, as shown in Figure 3(d), have also been observed in [100]- and [111]-oriented $Al_{0.3}CrFeCoNi$ micropillars.

3.4 TEM observation of the deformed nanopillars

To reveal the deformation mechanisms at different temperatures, we conducted detailed TEM observations of the compressed micropillars. Figure 4 shows a series of TEM images and associated selected area electron diffraction (SAED) patterns of the [100]-oriented $Al_{1.2}CrFeCoNi$ micropillars at different temperatures. At room temperature, a high density of dislocations accumulates in some regions (Figure 4(a)), indicating that dislocation tangles operate in the micropillars. However, the regions for dislocation accumulation still have a nearly perfect BCC lattice, as evidenced by the SAED pattern in Figure 4(c). Notably, dislocation cell structures occur in some regions in Figure 4(a), as shown in Figure 4(b). The SAED pattern in Figure 4(d) shows that these cell structures have a small misorientation. Similar cell structures of dislocations and even some subgrains with large misorientations are observed in [110]- and [111]-oriented micropillars at room temperature, as shown in Figures 5(a)–(c) and 6(a)–(c). This indicates that dynamic recrystallization (DRX) initiates in micropillars at 300 K. For micropillars compressed at 550 K, many subgrains are distributed over a wide and large region, as shown in Figure 4(e) and (f). These subgrains have a mean grain size of about 100 nm. The diffraction pattern (Figure 4(h)) shows that there is a misorientation of approximately 10° between several typical subgrains in Figure 4(h). These subgrains actually evolved from dislocation cell structures. A similar phenomenon is shown in [110]- and [111]-oriented micropillars at 550 K, as shown in Figures 5(d)–(f) and 6(d)–(f), respectively. This implies that DRX develops further in micropillars at 550 K compared to that in micropillars at 300 K. For micropillars at 675 K, nearly all regions in the micropillar are full of subgrains with a mean grain size of about 100 nm. It is clearly observed that a slip band travelled through the top micropillar, leading to the formation of a surface step. Such shear

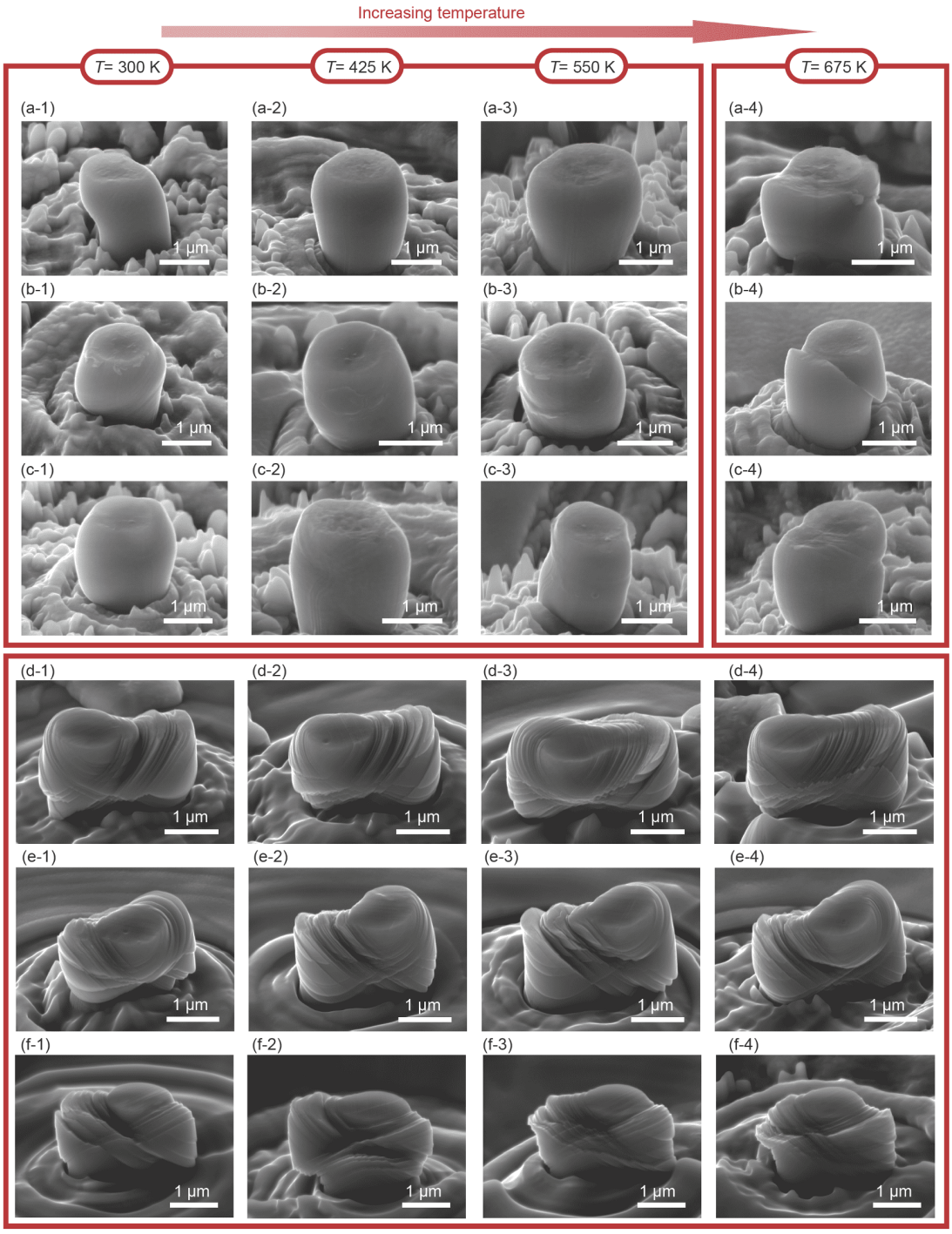

Figure 3 (Color online) Deformation morphologies of the $Al_{1.2}CrFeCoNi$ and $Al_{0.3}CrFeCoNi$ micropillars at different temperatures. (a) SEM images of the [100]-oriented $Al_{1.2}CrFeCoNi$ micropillars at different temperatures; (b) SEM images of the [110]-oriented $Al_{1.2}CrFeCoNi$ micropillars at different temperatures; (c) SEM images of the [111]-oriented $Al_{1.2}CrFeCoNi$ micropillars at different temperatures; (d) SEM images of the [110]-oriented $Al_{0.3}CrFeCoNi$ micropillars at different temperatures; (e) SEM images of the [100]-oriented $Al_{0.3}CrFeCoNi$ micropillars at different temperatures; (f) SEM images of the [111]-oriented $Al_{0.3}CrFeCoNi$ micropillars at different temperatures.

localization is due to massive dislocation slip occurring on particular slip planes at high temperatures. The shear localization is very pronounced in the [110]-oriented micropillars compressed at 675 K (Figure 5(g)–(i)). Notably, the localized shear band contains a number of elongated subgrains with a misorientation of about 15°, as shown in Figure 5(g)–(i).

The TEM images in Figures 4–6 revealed that during compression of the $Al_{1.2}CrFeCoNi$ micropillars, DRX occurs at temperatures from 300 K to 675 K, but shear localization is activated at 675 K. In the following parts, we further

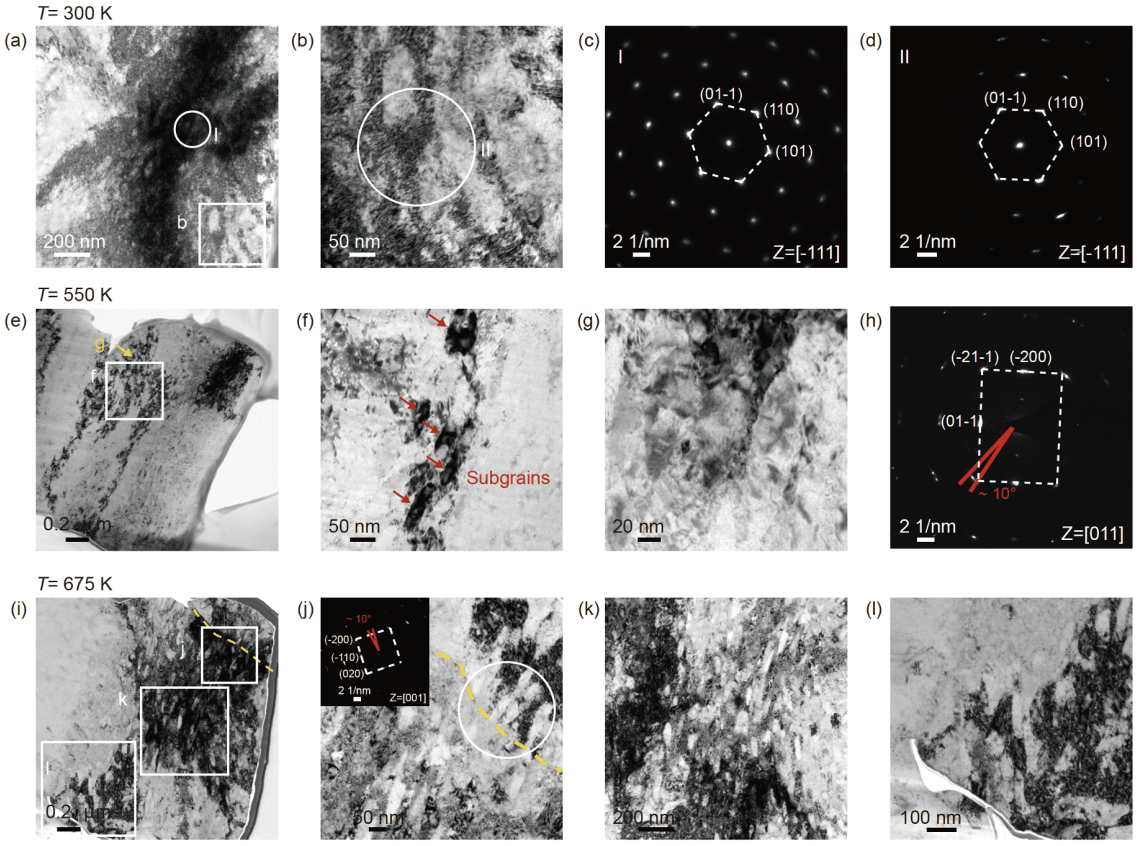

Figure 4 (Color online) Representative TEM images and associated SAED analyses of the [100]-oriented $Al_{1.2}CrFeCoNi$ micropillars at different temperatures. (a)–(d) 300 K; (e)–(h) 550 K; (i)–(l) 675 K. The arrows in (f) represent several subgrains. Three subgrains with a mean grain size of about 80 nm are shown in (g). (h) The corresponding SAED of (g) that shows that the misorientation of two subgrains is measured to be about 10°. (j)–(l) The presence of a wide range of subgrains. The surface step at the top of (i) implies that the dashed lines in (i) and (j) represent the slip directions for the dislocations. The inset in (j) indicates a misorientation of about 10° between the two sides of the slip line.

analyzed the DRX process and correlated the DRX process with the temperature insensitivity of the yield stress and even the increasing flow stress with increasing temperature. Previous studies [35] have shown that for metallic materials, there are two types of DRX during deformation: discontinuous dynamic recrystallization (dDRX) during hot working, where two steps (including the nucleation and growth of new grains) are discontinuous; and continuous dynamic recrystallization (cDRX) during severe plastic deformation, which is a so-called one-step process and occurs at low temperatures. At temperatures above $0.5T_m$, both cDRX and dDRX can occur simultaneously, but dDRX becomes dominant as the temperature rises [35,36]. When the temperature is below $0.5T_m$, only cDRX occurs, and dDRX is generally suppressed [35,36]. Note that the melting point of $Al_{1.2}CoCrFeNi$ was measured experimentally as 1643 K [14]; thus, the test temperature in our current experiment is lower than $0.5T_m$; therefore, the DRX that occurs in the $Al_{1.2}CrFeCoNi$ micropillars is actually cDRX.

By considering the TEM images at different temperatures, our TEM observations (Figures 4–6) actually indicate that the cDRX process occurs during compression of the $Al_{1.2}CrFeCoNi$ micropillars. In the single-crystal BCC micro/nanopillars, due to the relatively complex slip systems, dislocations prefer to interact, get tangled with each other and even self-multiply, leading to a high dislocation density (see Figure 4(a)) and resultant dislocation forest hardening [37]. With dislocation accumulation, cellular structures gradually form (Figure 4(b)) and then impede subsequent dislocation motion, facilitating an increase in the stress. As the plastic strain increases, the cell structures evolve into subgrains with small misorientations (Figure 4(e) and (i)). The misorientations between neighboring subgrains progressively increase with the accumulation of additional dislocations [35]. As the test temperature increases, the cDRX process described above becomes pronounced because additional dislocations are thermally activated. Therefore, the micropillars compressed at high temperatures contain additional subgrains. The cDRX process indicated by our TEM observation is similar to dynamic nanocrystallization in some BCC metals during severe plastic deformation [35]. However, it is noted that the misorientations of subgrains formed in our BCC HEA micro-pillars are smaller than those of subgrains formed in BCC metals under severe plastic

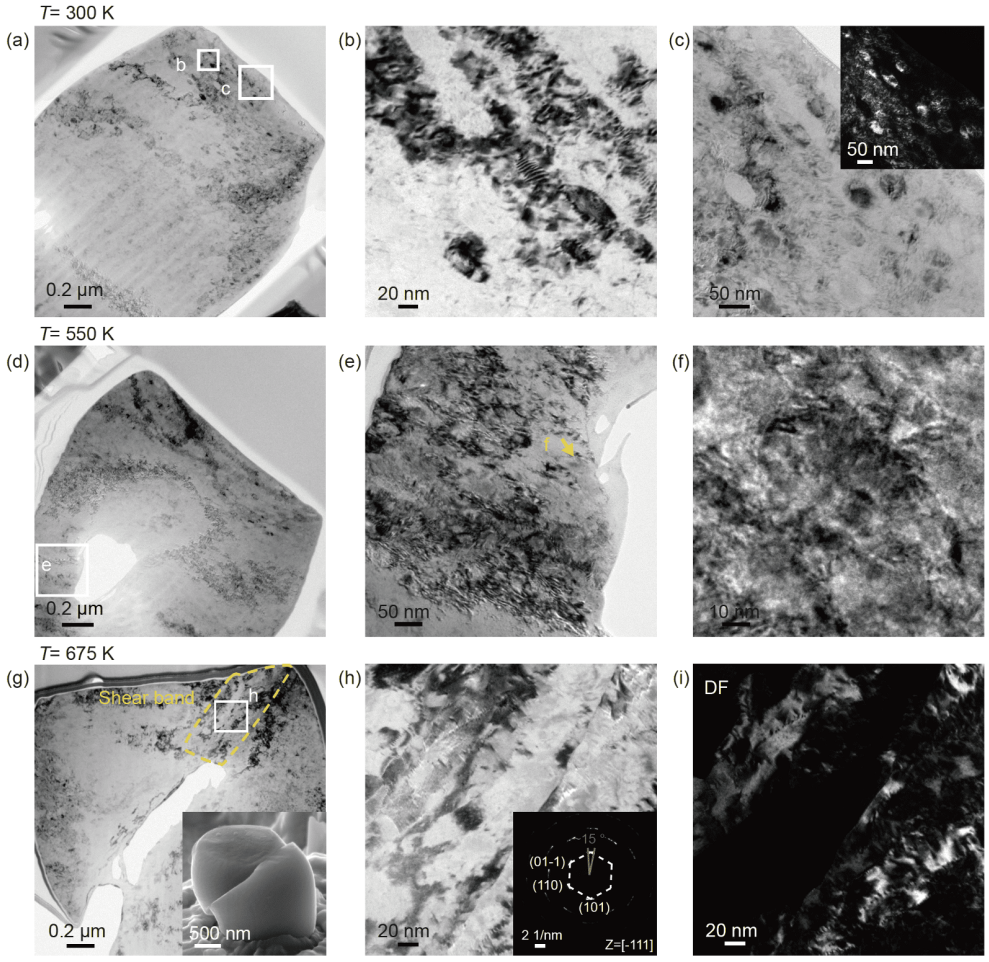

Figure 5 (Color online) Representative TEM images of [110]-oriented $Al_{1.2}CrFeCoNi$ single-crystal micropillars at different temperatures. (a)–(c) 300 K; (d)–(f) 550 K; (g)–(i) 675 K. (f) shows a sub-grain with the size of about 100 nm in the region labeled by 'f' in (e). In (h), several elongated sub-grains with misorientation of about 15° are in a micro-sized shear in (g).

deformation [35], which is related to the difference in the extent of plastic deformation. Furthermore, it is noted that the cDRX occurs during compression of $Al_{1.2}CrFeCoNi$ micropillars. Such cDRX is associated with dislocation accumulation and tangle at the large plastic strain under compression. Compared with the compressive deformation, the BCC $Al_{1.2}CrFeCoNi$ under tensile deformation has the smaller fracture strain. Thus, the BCC $Al_{1.2}CrFeCoNi$ micropillars might fail at the small strain and cannot sustain large plastic strain during tension. As a result, the cDRX might not be observed during the tension of $Al_{1.2}CrFeCoNi$ micropillars.

Essentially, the cDRX process is a grain refinement process. In our experiments herein, the microsized grain interior of the pillar is gradually separated into many nanosized grains with increasing misorientation as the plastic strain increases. These nanosized grains or their grain boundaries further confine and block dislocation motion, facilitating an increase in the flow stress. At the same time, the increasing fraction and misorientation of nanosized grains also contributes to an increase in the stress. Such strengthening due to cDRX has been demonstrated in previous experimental studies [35]. As the tested temperature increases, the cDRX becomes pronounced, and the associated strengthening becomes very prominent. Therefore, such strengthening from cDRX competes with the thermal softening and significantly reduces the temperature dependence of the yield and flow stresses, which causes the temperature insensitivity of the yield stress, increases the flow stress with increasing temperature, and increases the work hardening rate with increasing temperature.

For comparison, we also investigated the deformation mechanisms of $Al_{0.3}CrFeCoNi$ micropillars at different temperatures by conducting TEM analyses. Figure 7 shows representative TEM images and relevant SAED patterns of the compressed $Al_{0.3}CrFeCoNi$ micropillars with three orientations. Figure 7(a) and its inset show the typical dislocation structures. Regardless of the orientation and temperature, a high density of nanoscale twins is observed in all the $Al_{0.3}CrFeCoNi$ micropillars, as shown in Figure 7(a)–

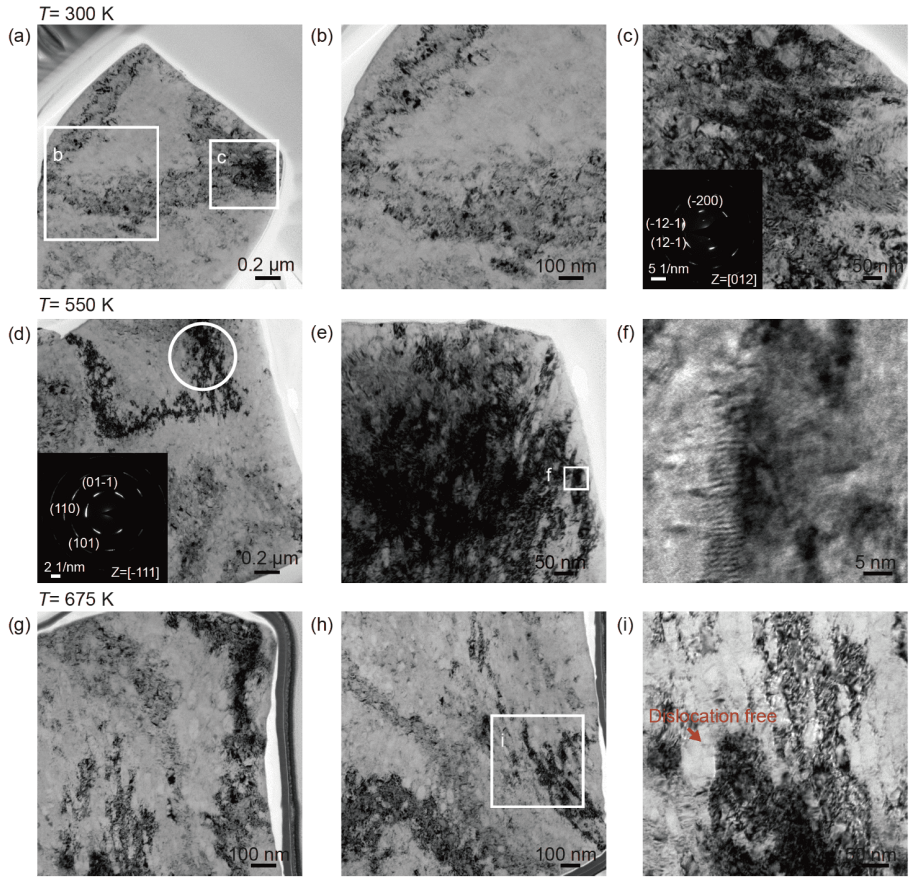

Figure 6 (Color online) Representative TEM images of [111]-oriented $Al_{1.2}CrFeCoNi$ single-crystal micropillars at different temperatures. (a)–(c) 300 K; (d)–(f) 550 K; (g)–(i) 675 K. The arrow in (i) shows a well-formed sub-grain which is almost dislocation free.

(o). For the [110]-oriented micropillars compressed at 300 K, there are even nanoscale twins intersecting with each other, as indicated by Figure 7(h)–(l). These TEM observations imply that during compression of the $Al_{0.3}CrFeCoNi$ micropillars with all three orientations, deformation twinning is always a dominant mechanism at both room temperature and elevated temperatures. For FCC metals/alloys, deformation twinning is induced by continuous slip of Shockley partial dislocations on the same slip plane [38]. The activation of deformation twinning is mainly determined by the stacking fault energy (SFE). The lower the SFE is, the more easily deformation twinning is activated. $Al_{0.3}CrFeCoNi$ has a relatively low SFE of 51 mJ m^{-2} [39,40]. Previous experimental studies have shown that deformation twinning is prevalent during compression of the $Al_{0.3}CrFeCoNi$ bulk sample [40]. These results further confirmed our conclusion from the TEM observations. In FCC metals/alloys, deformation twinning generally prefers to occur at low temperatures, while dislocation slip prefers high temperatures due to the presence of thermal activation [15,41,42]. Therefore, as the temperature increases, thermally activated dislocation slip becomes pronounced and easy, while deformation twinning gradually decreases, leading to a decrease in the yield and flow stresses with increasing temperature. This provides a rational explanation for the apparent thermal softening in $Al_{0.3}CrFeCoNi$ micropillars. Furthermore, it is noted that in our current study, the deformation twinning is a dominant mechanism during compression of $Al_{0.3}CrFeCoNi$ micropillars, while the dynamic recrystallization due to the dislocation slip and tangle is a controlling mechanism during compression of $Al_{1.2}CrFeCoNi$ micropillars. It implies that the $Al_{1.2}CrFeCoNi$ system might have a higher SFE than the $Al_{0.3}CrFeCoNi$ system.

4 Conclusion

In summary, we have conducted *in situ* SEM compression of $Al_{1.2}CrFeCoNi$ (comprising the BCC phase) and $Al_{0.3}CrFeCoNi$ (comprising the FCC phase) single-crystal micropillars with three orientations at temperatures varying from 300 K to 675 K. The experimental results showed that the yield stresses of the $Al_{1.2}CrFeCoNi$ micropillars are insensitive to increasing temperature, and their flow stresses and work hardening rates increase as the temperature increases from 300 K to 550 K. In comparison, the yield

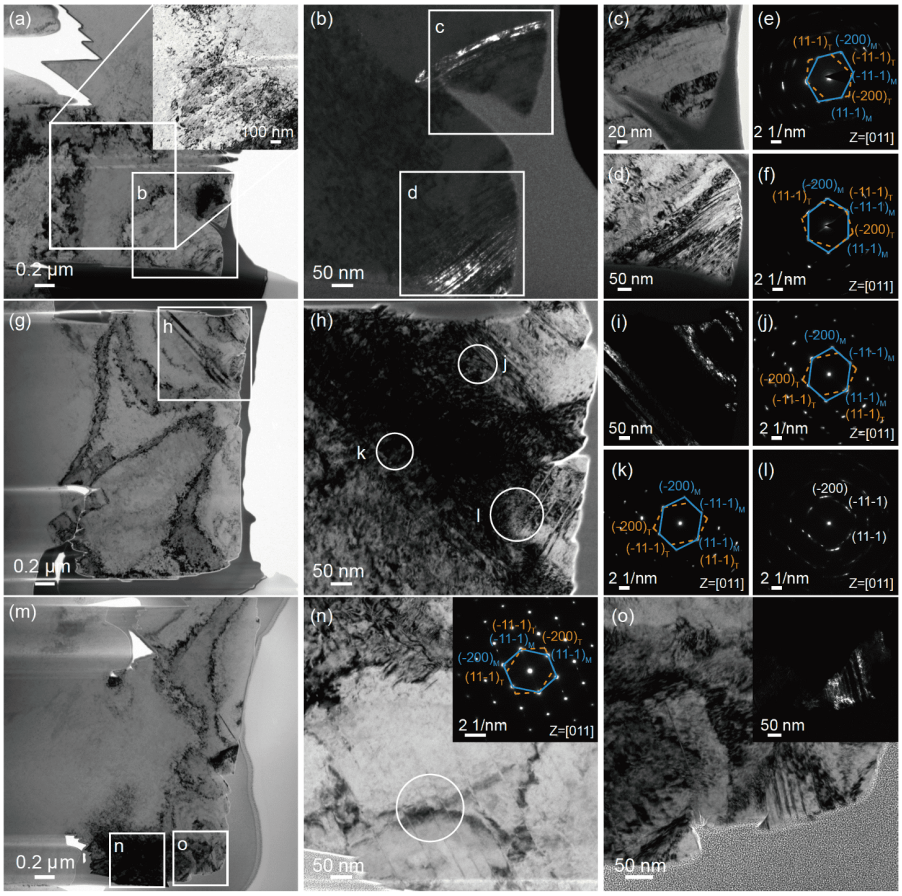

Figure 7 (Color online) Representative TEM images and associated SAED analyses of the $Al_{0.3}CrFeCoNi$ single-crystal micropillars with different orientations at different temperatures. (a)–(f) [100] orientation at 675 K; (g)–(l) [110] orientation at 300 K; (m)–(o) [111] orientation at 675 K. The inset in (a) is a magnified view of the boxed region in (a). (b) The dark-field image of the boxed region labeled by 'b' in (a). (c), (d) The magnified images of the boxed region in (b), and (e), (f) show the corresponding SAED of (c) and (d). (i) The dark-field image of (h), and (j)–(l) show the SAED of the circled regions labeled 'j', 'k' and 'l'. (i)–(l) Image showing that a high density of nanoscale twins along two directions intersect with each other in (h). (n)–(o) Magnified images of the boxed regions in (m). The inset in (n) shows the SAED of the circled region in (n). The inset in (o) shows the corresponding dark field of (o). These figures indicate that deformation twinning is a dominant mechanism in the $Al_{0.3}CrFeCoNi$ single-crystal micropillars.

stresses of the $Al_{0.3}CrFeCoNi$ micropillars decrease with increasing temperature and exhibit typical thermal softening. Detailed TEM analyses further revealed that for the $Al_{1.2}CrFeCoNi$ micropillars, the temperature insensitivity of the yield stress and increasing flow stress (and work hardening rate) with increasing temperature originate from the DRX process due to the tangle and accumulation of a large number of dislocations during compression. For the $Al_{0.3}CrFeCoNi$ micropillars, the thermal softening can be related to thermally activated dislocation slip. The SEM observations showed that the $Al_{1.2}CrFeCoNi$ micropillars exhibit a transition from homogenous deformation to shear localization as the temperature increases, while the $Al_{0.3}$-$CrFeCoNi$ micropillars always maintain a well-distributed and fine slip deformation process at all test temperatures due to dislocation nucleation from the surface and multiple slip systems. Our current study not only contributes to a more comprehensive understanding of the temperature dependence of plasticity in BCC HEAs, but can also provide guidance for the design and fabrication of HEAs used for thermomechanical devices and structures, as well as the design of more reliable high temperature alloys used in aerospace engineering.

Li XiaoYan gratefully acknowledges the financial support from the National Natural Science Foundation of China (Grant Nos. 11522218, 11720101002), the Beijing Natural Science Foundation (Grant No. Z180014) and the National Science and Technology Major Project (Grant No. 2017-VI-0003-0073). Gao HuaJian acknowledges financial support from the National Science Foundation (Grant No. DMR-1709318).

1 Ding Q, Zhang Y, Chen X, et al. Tuning element distribution, structure and properties by composition in high-entropy alloys. Nature, 2019, 574: 223–227
2 Zhang Z J, Mao M M, Wang J, et al. Nanoscale origins of the damage tolerance of the high-entropy alloy CrMnFeCoNi. Nat Commun, 2015, 6: 1–6
3 Zhang Y, Zuo T T, Tang Z, et al. Microstructures and properties of high-entropy alloys. Prog Mater Sci, 2014, 61: 1–93
4 Giwa A M, Liaw P K, Dahmen K A, et al. Microstructure and small-scale size effects in plasticity of individual phases of $Al_{0.7}CoCrFeNi$

high entropy alloy. Extreme Mech Lett, 2016, 8: 220–228
5 Yeh J W, Chen S K, Lin S J, et al. Nanostructured high-entropy alloys with multiple principal elements: Novel alloy design concepts and outcomes. Adv Eng Mater, 2004, 6: 299–303
6 Cantor B, Chang I T H, Knight P, et al. Microstructural development in equiatomic multicomponent alloys. Mater Sci Eng-A, 2004, 375-377: 213–218
7 Yeh J W. Recent progress in high-entropy alloys. Ann Chim Sci Mat, 2006, 31: 633–648
8 Li Z, Zhao S, Ritchie R O, et al. Mechanical properties of high-entropy alloys with emphasis on face-centered cubic alloys. Prog Mater Sci, 2019, 102: 296–345
9 Tang Z, Yuan T, Tsai C W, et al. Fatigue behavior of a wrought $Al_{0.5}$CoCrCuFeNi two-phase high-entropy alloy. Acta Mater, 2015, 99: 247–258
10 Zhang H, Wing Siu K, Liao W, et al. *In situ* mechanical characterization of CoCrCuFeNi high-entropy alloy micro/nano-pillars for their size-dependent mechanical behavior. Mater Res Express, 2016, 3: 094002
11 Ding Q, Fu X, Chen D, et al. Real-time nanoscale observation of deformation mechanisms in CrCoNi-based medium- to high-entropy alloys at cryogenic temperatures. Mater Today, 2019, 25: 21–27
12 Kao Y F, Chen T J, Chen S K, et al. Microstructure and mechanical property of as-cast, -homogenized, and -deformed Al_xCoCrFeNi ($0 \le x \le 2$) high-entropy alloys. J Alloys Compd, 2009, 488: 57–64
13 Wang W R, Wang W L, Wang S C, et al. Effects of Al addition on the microstructure and mechanical property of Al_xCoCrFeNi high-entropy alloys. Intermetallics, 2012, 26: 44–51
14 Wang W R, Wang W L, Yeh J W. Phases, microstructure and mechanical properties of Al_xCoCrFeNi high-entropy alloys at elevated temperatures. J Alloys Compd, 2014, 589: 143–152
15 Gludovatz B, Hohenwarter A, Catoor D, et al. A fracture-resistant high-entropy alloy for cryogenic applications. Science, 2014, 345: 1153–1158
16 Liang R, Khan A S. A critical review of experimental results and constitutive models for BCC and FCC metals over a wide range of strain rates and temperatures. Int J Plast, 1999, 15: 963–980
17 Voyiadjis G Z, Abed F H. Microstructural based models for bcc and fcc metals with temperature and strain rate dependency. Mech Mater, 2005, 37: 355–378
18 Cui Y, Po G, Ghoniem N. Temperature insensitivity of the flow stress in body-centered cubic micropillar crystals. Acta Mater, 2016, 108: 128–137
19 Senkov O N, Wilks G B, Scott J M, et al. Mechanical properties of $Nb_{25}Mo_{25}Ta_{25}W_{25}$ and $V_{20}Nb_{20}Mo_{20}Ta_{20}W_{20}$ refractory high entropy alloys. Intermetallics, 2011, 19: 698–706
20 Miracle D B, Senkov O N. A critical review of high entropy alloys and related concepts. Acta Mater, 2017, 122: 448–511
21 Greer J R, Weinberger C R, Cai W. Comparing the strength of fcc and bcc sub-micrometer pillars: Compression experiments and dislocation dynamics simulations. Mater Sci Eng-A, 2008, 493: 21–25
22 Tung C C, Yeh J W, Shun T, et al. On the elemental effect of AlCoCrCuFeNi high-entropy alloy system. Mater Lett, 2007, 61: 1–5
23 Zou Y, Wheeler J M, Ma H, et al. Nanocrystalline high-entropy alloys: A new paradigm in high-temperature strength and stability. Nano Lett, 2017, 17: 1569–1574
24 Brinckmann S, Kim J Y, Greer J R. Fundamental differences in mechanical behavior between two types of crystals at the nanoscale. Phys Rev Lett, 2008, 100: 155502
25 Kim J Y, Jang D, Greer J R. Insight into the deformation behavior of niobium single crystals under uniaxial compression and tension at the nanoscale. Scripta Mater, 2009, 61: 300–303
26 Couzinié J P, Dirras G. Body-centered cubic high-entropy alloys: From processing to underlying deformation mechanisms. Mater Charact, 2018, 147: 533–544
27 Sestak B, Seeger A. Glide and work-hardening in bcc metals and alloys. II. Z Metallkde, 1978, 69: 355–363
28 Hagen A B, Snartland B D, Thaulow C. Temperature and orientation effects on the deformation mechanisms of α-Fe micropillars. Acta Mater, 2017, 129: 398–407
29 Kunz A, Pathak S, Greer J R. Size effects in Al nanopillars: Single crystalline vs. bicrystalline. Acta Mater, 2011, 59: 4416–4424
30 Wu Z, Bei H, Pharr G M, et al. Temperature dependence of the mechanical properties of equiatomic solid solution alloys with face-centered cubic crystal structures. Acta Mater, 2014, 81: 428–441
31 Schneider A S, Kaufmann D, Clark B G, et al. Correlation between critical temperature and strength of small-scale bcc pillars. Phys Rev Lett, 2009, 103: 105501
32 Abad O T, Wheeler J M, Michler J, et al. Temperature-dependent size effects on the strength of Ta and W micropillars. Acta Mater, 2016, 103: 483–494
33 Seeger A. Peierls barriers, kinks, and flow stress: Recent progress. MEKU, 2002, 93: 760–777
34 Argon A. Strengthening Mechanisms in Crystal Plasticity. Toronto: Oxford University Press, 2007. 78–133
35 Sakai T, Belyakov A, Kaibyshev R, et al. Dynamic and post-dynamic recrystallization under hot, cold and severe plastic deformation conditions. Prog Mater Sci, 2014, 60: 130–207
36 Guo N N, Wang L, Luo L S, et al. Hot deformation characteristics and dynamic recrystallization of the MoNbHfZrTi refractory high-entropy alloy. Mater Sci Eng-A, 2016, 651: 698–707
37 Weinberger C R, Cai W. Surface-controlled dislocation multiplication in metal micropillars. Proc Natl Acad Sci USA, 2008, 105: 14304–14307
38 Christian J W, Mahajan S. Deformation twinning. Prog Mater Sci, 1995, 39: 1–157
39 Kireeva I V, Chumlyakov Y I, Pobedennaya Z V, et al. Orientation and temperature dependence of a planar slip and twinning in single crystals of $Al_{0.3}$CoCrFeNi high-entropy alloy. Mater Sci Eng-A, 2018, 737: 47–60
40 Ma S G, Zhang S F, Gao M C, et al. A successful synthesis of the CoCrFeNi$Al_{0.3}$ single-crystal, high-entropy alloy by Bridgman solidification. JOM, 2013, 65: 1751–1758
41 Zhang Z, Sheng H, Wang Z, et al. Dislocation mechanisms and 3D twin architectures generate exceptional strength-ductility-toughness combination in CrCoNi medium-entropy alloy. Nat Commun, 2017, 8: 1–8
42 Li D, Li C, Feng T, et al. High-entropy $Al_{0.3}$CoCrFeNi alloy fibers with high tensile strength and ductility at ambient and cryogenic temperatures. Acta Mater, 2017, 123: 285–294